www.sciencemag.org/cgi/content/full/science.aaf1084/DC1

Supplementary Material for

Translation dynamics of single mRNAs in live cells and neurons

Bin Wu, Carolina Eliscovich, Young J. Yoon, Robert H. Singer*

*Corresponding author. Email: robert.singer@einstein.yu.edu

Published 5 May 2016 as *Science* First Release
DOI: 10.1126/science.aaf1084

This PDF file includes:

Other Supplementary Material for this manuscript includes the following:
(available at www.sciencemag.org/content/science.aaf1084/DC1)

Supporting Online Material for

Translation Dynamics of Single mRNAs in Live Cells and Neurons

Bin Wu[1,2], Carolina Eliscovich[1], Young J. Yoon[1] and Robert H. Singer[1,2,3*]

[1]Department of Anatomy and Structural Biology, [2]Gruss-Lipper Biophotonics Center,
Albert Einstein College of Medicine, Bronx, NY 10461

[3] Janelia Research Campus, Howard Hughes Medical Institute

*To whom correspondence should be addressed. E-mail: robert.singer@einstein.yu.edu

Contents

1. Materials and Methods

Plasmids and viral transduction

All lentiviral constructs were cloned into the phage-ubc-RIG lentiviral vector (*40*), from which the DsRed-IRES-GFP fragement had been excised and replaced with the constructs made in house. For the SINAPS constructs, we created tag-24xSuntagV4-oxBFP-AID, where tag could be flag or CytERM. The 24xSuntagV4 was amplified by polymerase chain reaction (PCR) from pcDNA4TO-24xGCN4_v4-sfGFP (Addgene #61058) (*16*). The oxBFP and CytERM sequences were kind gifts from Erik L. Snapp (*21*). AID was PCRed form pcDNA5-H2B-AID-EYFP (Addgene #47329) (*19*). In the 3'UTR, we have inserted 24xMBSV5 (*22*) right before the woodchuck hepatitis virus posttranscriptional regulatory element (WPRE) in the lentiviral backbone. Between MBS and the stop codon, we inserted the 3'UTR (nucleotide 1-441) of mouse β-actin mRNA. To vary the length of the transcript, we excised oxBFP or replaced it with firefly luciferase (Fluc, 1650nt) or Fluc-oxBFP (2388 nt). For MS2 coat protein, we used the synonymously transformed stdMCP-tagRFP-T, stdMCP-Halotag (Promega) or stdMCP-stdGFP (*22*). Lentiviral particles were produced by transfecting the expression vector with accessory plasmids, ENV, REV, VSVG and GAG in 293T cells. Collected lentiviral particles were purified with lenti-X concentrator (Clontech, Mountain View, CA).

The plasmid pBabe-TIR1-9myc was obtained from Addgene (Addgene #47328) (*19*). To make retroviral particles, we transfected the pBabe vector, VSVG and pGag-Pol in GP2-293 cells (Clontech, Mountain View, CA). The supernatant was collected and the retroviral particles were purified with Lenti-X concentrator with the retroviral harvesting protocol from manufacturer (Clontech, Mountain View, CA). The plasmid phR-scFV-GCN4-sfGFP-GB1-NLS-dWPRE was also obtained from Addgene (Addgene #60906) (*16*). To combine the OsTIR1 and scFV-sfGFP into one plasmid, we used the phage-ubc-DsRed-IRES-GFP backbone. We replaced DsRed before the IRES with OsTIR1-myc, and GFP after the IRES with scFV-GCN4-sfGFP-GB1. Note we removed the nuclear localization signal (NLS) in the scFV-GCN4-sfGFP-GB1 construct. The lentiviral particles for these plasmids were produced as previously described.

Stable U2OS cell lines

Human U2OS osteoscarcoma cell line (American Type Culture Collection HTB-96) was grown at 37°C and 5% CO_2 in DMEM containing 4.5g/L glucose, 10% FBS and 1% penicillin-streptomycin. To make stable U2OS cell lines expressing MCP, we infected the cells with stdMCP-tagRFP-T, stdMCP-Halotag or stdMCP-stdGFP lentivirus. We selected positive cells with low expressions by fluorescence activated cell sorting (FACS). The cells were then infected with pBabe-TIR1-9myc retrovirus and followed drug selection by 5 μg/mL puromycin for a week. Single colonies of the cells were cultured. The clone that expresses a high level of TIR1-9myc was chosen for further experiments. The cell line was then infected with phR-scFV-GCN4-sfGFP-GB1-NLS-dWPRE and followed by FACS to select positive GFP cells. Finally, the cells expressing all three plasmids, stdMCP, OsTIR1 and scFV-sfGFP, were infected with SINAPS reporters. We used the polyclonal stable SINAPS cell lines for the experiments if not stated otherwise.

Culture of primary hippocampal neurons from mouse

Post-natal day 1 (P1) mouse hippocampal tissue were isolated from C57BL6 WT pups. Hippocampi were placed in 0.25% trypsin for 15 minutes at 37 °C. Tissue was triturated and plated onto Poly-D-lysine (Sigma) coated glass-bottom dishes (Matek) at 75,000 cells per dish and cultured in Phenol red free Neurobasal A media supplemented with B-27, GlutaMax and primocin (InvivoGen). Neurons were imaged between 2-3 weeks in culture. For live imaging of neurons, the Matek dish containing cultured neurons were directly moved from incubator to the microscope stage incubator with the original culture medium. The neurons were kept in stage incubator at 35-37 °C with 5% CO_2 when imaging. For FISH & IF experiment, the neurons were fixed between 2-3 weeks in culture. All reagents for neuron culture were acquired from Life Technologies unless noted otherwise.

Sample preparation and live cell fluorescence imaging

The U2OS cells stably expressing stdMCP-Halotag, Os-TIR1, scFV-sfGFP and SINAPS constructs were plated the day before imaging. Indole-3-acetic acid (IAA) (I3750, Sigma-Aldrich) (250mg/mL in ethanol) was diluted into the cell culture (final concentration 500 μg/mL) to degrade the pre-existing proteins containing auxin-induced-degron. To label stdMCP-Halotag, the cells were incubated in medium containing 1nM Halo-JF549 dyes for 30 minutes. After washing 3 times with warm medium, the cells were further incubated in normal medium for 30 minutes to wash out the residual dyes. When imaging, the medium was changed to phenol red free Leibovitz-15 medium (Sigma Aldrich) and incubates on a stage incubator at 35-37 °C.

For neuron imaging, dissociated mouse hippocampal neurons were infected with lentivirus expressing OsTIR1-IRES-scFV-sfGFP and flag-SINAPS at DIV 7. Neurons were imaged between 2-3 weeks in culture. The neurons were kept in their original culture medium and incubated on microscope with 5% CO_2 at 35-37 °C. The neurons were also treated with 500 μg/mL IAA overnight before imaging to degrade the existing proteins.

Single molecule fluorescence in situ hybridization & immunofluorescence

The detailed protocol for single molecule FISH & IF is described in Eliscovich et al (submitted). Briefly, the cells were fixed, permeabilized, and incubated with 100 nM of MS2V5 and 100 nM of SuntagV4 labeled mix probe sets (Stellaris RNA FISH probes, Biosearch Technologies) and primary antibody against GFP (GFP-1010, from Aves Labs, Inc) for 3 hours at 37°C. After wash, the cells were incubated with Alexa Fluor 647 secondary antibody (Life Technologies) and mounted using ProLong diamond antifade reagent with DAPI (Life Technologies). Images were taken in a custom up-right wide-field Olympus BX-63 microscope equipped with an X-Cite 120 PC lamp (EXFO), ORCA-R2 Digital CCD camera (Hamamatsu), SuperApochromatic 60x/1.35 NA Olympus objective (UPLSAPO60XO) and zero pixel shift filter sets: DAPI-5060C-Zero, Cy3-4040C-Zero and Cy5-4040C-Zero (Semrock). Image pixel size: XY, 107.5 nm; Z-steps, 200 nm. The FISH probes are listed in the supplementary table I.

Fluorescence microscopy

The two-color simultaneous imaging of mRNA and translation sites was performed on a modified version of the home-built microscope described in (*27*). Briefly, the microscope was built around an IX71 stand (Olympus). For excitation, a 491nm laser (Calypso^{TM} , Cobolt) and a 561nm laser

(Jive™ , Cobolt) were combined and controlled by an acoustic-optic tunable filter (AOTF, AOTFnC-400.650-TN, AA Opto-electronic) before coupled into a single mode optical fiber (Qioptiq). The output of the fiber was collimated and delivered through the back port of the microscope and reflected into an Olympus 150x 1.45 N.A. oil immersion objective lens with a dichroic mirror (zt405/488/561rpc, 2mm substrate, Chroma). The tube lens (180mm focal length) was removed from the microscope and placed outside of the right port. A triple band notch emission filter (zet405/488/561m) was used to filter the scattered laser light. A dichroic mirror (T560LPXR, 3mm substrate, Chroma) was used to split the fluorescence onto two precisely aligned EMCCDs (Andor iXon3, Model DU897) mounted on alignment stages (x, y, z, θ- and ϕ- angle). Emission filters FF03-525/50-25 and FF01-607/70-25 (Semrock) were placed in front of green and red channel cameras respectively. The two cameras were triggered for exposure with a TTL pulse generated on a DAQ board (Measurement Computing). The microscope was equipped with a piezo stage (ASI) for fast z-stack and a Delta-T incubation system (Bioptech) for live cell imaging. The microscope (AOTF, DAQ, Stage and Cameras) was automated with the software Metamorph (Molecular Devices). For two-color live cell imaging, the U2OS cells were streamed at 50 ms in a single plane.

The single translation site FRAP experiment was performed on a fluorescence microscope built around an IX-81 stand (Olympus). The back port of the microscope was removed to allow custom laser illumination. For excitation of fluorescent proteins, a 491 nm laser (Calypso-25, Cobolt, San Jose, CA), a 561 nm line (LASOS-561-50, Lasertechnik GmbH, Germany) and a 640 nm line (CUBE 640-40C, Coherent Inc, Santa Clara, CA) were combined, expanded and delivered through the back port. A size-adjustable iris was used to limit the illumination to an area of approximately 80 μm in diameter. The lasers were reflected by a four-band excitation dichroics mirror (Di01-R405/488/561/635, Semrock) to a 150x 1.45 N.A. oil immersion objective (Olympus). The fluorescence was collected by the same objective, passed through the dichroic mirror, a notch filter (NF01-405/488/561/635, Semrock), emission filters and were recorded on an EMCCD camera (Andor, iXon3 DU-897E-CS0-#BV). The emission filters (FF01-525/50 for green and FF01-605/64 (Semrock) for red respectively) were mounted on a motorized filter wheel (FW-1000, Applied Scientific Instrumentation) for fast switching between wavelengths. To bleach a single translation site with diffraction limited illumination, the 491 nm laser was collimated by a lens before entering the objective. Switching between the diffraction-limited and wide-field illumination was achieved by flipping the collimating lens (Thorlabs AC254-150-A, L3) in and out of the light path via a motorized flipping mount (Thorlabs, MFF001). All laser power and shuttling were controlled by an acousto-optic tunable filter (AOTF) (AOTFnC-400.650-TN, AA Opto-electronic). The microscope was also equipped with an automated XY-stage (ASI, MS2000-XY with extra fine lead-screw pitch of 0.635 mm and a 10 nm linear encoder resolution) and a piezo-Z stage (ASI) for fast *z*-stack acquisition. The AOTF, flipping mount, piezo-stage were all controlled by a DAQ board (DaqBoard/2001, IOTech, Inc). The cells were kept at 37°C with a stage top incubator (INUBH-ZILCS-F1, Tokai Hit, Japan). The microscope was controlled with the imaging software Metamorph (Molecular Devices, Sunnyvale, CA). The FRAP procedure was automated with custom journals in Metamorph. Briefly, the focused 491nm laser position was recorded in advance in Metamorph. The translation site was moved to the laser spot and two pre-bleaching images were taken. The illumination was changed to focused 491nm laser illumination for two seconds to bleach the single translation site at the focus. Then the illumination was

switched immediately back to wide-field illumination. The post-bleaching images were taken every 10 seconds. All FRAP images (both pre and post) were 7-slice z-stacks with 500 nm distance between slices. The z-stacks were maximum-projected before analysis.

Image analysis

FISH & IF analysis

FISH&IF images were analyzed using FISH Quant (*41*). Briefly, after background subtraction, the FISH spots in the cytoplasm were fit to a 3D Gaussian to determine the coordinates of the mRNA in each color. The intensity and the width of the 3D Gaussian were thresholded to exclude autofluorescent particles and non-specific signals. For colocalization analysis, the mRNA and Suntag signals were first determined by FISH Quant independently. To find translation sites colocalized with mRNA, we find the brightest Suntag spot within 300 nm of mRNA (*29*). To calculate the integrated intensity of single Suntag protein, we used the mean value of all spots that not colocalizing with mRNAs. The number of nascent peptides was derived by dividing the integrated intensity by that of the single protein. Since there were nascent peptides that had not been synthesized the full Suntag motif, the reported number of peptides was only the full-length equivalent. The number of ribosomes on the translation sites should be larger than the reported value. If a constitutive translation kinetic model was used as described in the Supplemental Theoretical Derivation, the correction factor could be readily calculated as $(1-(N-1)/2M$, where N=24 is the number of Suntag epitopes and M is the length of the ORF measured in the epitope size. For flag-24xSuntag-oxBFP-AID (M=44), the correction factor would be 0.74.

Tracking of mRNA and translation sites

All analysis was performed with existing software packages and custom built programs written in Matlab (MathWorks). For particle tracking, we used a combination of AirLocalize (*28*) and u-track (*29*). The positions of mRNA and TLS are calculated by AirLocalize. The detected particle positions for each frame were tracked with the program u-track respectively in each channel. Only tracks with more than 5 frames were used for the analysis. To find the mRNA and TLS moving toether, we first calculated the distances between all mRNA tracks and TLS tracks. The distance between tracks was defined as the mean distance between particle positions in overlapped frames. The TLS track with the minimum distance to the mRNA track was chosen as the co-moving track if the distance was smaller than a threshold value (0.53μm). The fraction of mRNA in translation was determined as the ratio between the number of mRNA tracks with a co-moving TLS and the total number of mRNA tracks. To calculate the diffusion coefficient of each track, we used the mean-square-displacement (MSD) and fit the first 7 values of MSD. The u-track program also classified the tracks as confined or freely diffusing. Furthermore, we classified mRNAs with diffusion coefficients less than 0.01μm^2/s as confined. For mRNA in each category, we calculated the fraction of translating mRNAs respectively.

FRAP analysis

The integrated intensity of the translation sites was obtained with the Gaussian mask algorithm used in AirLocalize (*28*). When the translation site was bleached after the pre-images, we used the position of the TLS determined in the pre-bleaching images to calculate intensity until the TLS reappeared. Afterwards, we used the newly emerged TLS position to calculate intensity. Since the mRNA was tethered to the ER, the TLS usually did not move much before appearing again close by. To correct

the FRAP curve due to the photo bleaching, the nuclear fluorescence intensity was fitted to a single exponential model to calculate the correction factor. The raw recovery curve was divided by the correction factor to account for photo bleaching. The recovery curves were normalized with the integrated intensity value of the TLS measured in the pre-bleaching images. A nonlinear least square fit (lsqcurvefit in Matlab) was used to fit the theoretical curve (Eq. 15) to the average recovery curve to determine the elongation rate and the error bar (nlparci in Matlab). Theoretical derivation of the FRAP curve was described in the Supplemental Theoretical Derivation. During the fit, the amplitude of the recovery was allowed to vary as a free parameter.

Fluctuation analysis of translation sites in neurons

To track translation sites in neurons, we chose mRNAs in dendrites (mostly >30 μm from soma or in secondary dendrites) where the translation sites were very sparse and easy to track (mostly 1 or 2). We used a Gaussian mask algorithm to find the position of translation sites and u-track program for assembling the particle trajectories. To account for the disappearance of translation sites, if no particle was found by the localization algorithm, the tracking procedure used the position when the particle was last found as the putative location to calculate the integrated intensity with the Gaussian mask algorithm. We used the measured integrated intensity value of the TLS to calculate the linear autocorrelation function. The theoretical autocorrelation function (Supplemental Theoretical Derivation) was fitted to the data with a nonlinear least square routine (lsqcurvefit in Matlab).

Western Blotting

We used the following antibodies to detect the BFP in the SINAPS and sfGFP in the scFV-sfGFP constructs: Roche mouse monoclonal anti-GFP, goat-anti-mouse IRDye800CW secondary antibody (Li-cor). The images were acquired on an Odyssey infrared imaging system.

2. Theoretical Derivation

Derivation of the FRAP theory for translation

The theory is based on the visualization of nascent peptides (NAP) using the Suntag technology. The epitope peptide of the single chain variable fragment (scFV) of the antibody GCN4 is multimerized and placed at the N-terminal of the translation reporter. As soon as the NAP emerges from the ribosome, the superfolder GFP (sfGFP) labeled scFV binds to it and makes it visible. The fluorescence intensity of translation site (TLS) depends on the number of NAPs, which in turn is determined by the enzymatic activity of ribosomes. Therefore, a kinetic model of ribosome activity is needed. The modeling here closely follows a similar theory for transcription by RNA polymerase II (*5*).

To simplify the description, we use an epitope peptide as the translation unit instead of a single codon. There are 24 amino acids in each Suntag eptitope including linker region. Suppose that the reporter contains *N* segments of Suntag epitopes at the N-terminal. The flag and CytERM before Suntag motif are neglected since they are not visualized. The whole reporter contains *M* epitope-size equivalent segments of amino acids. For example, each Suntag peptide has 24 amino acids including linker. In flag-SINAPS construct, there are 24 Suntag peptides in the N-terminal *N*=24. After Suntag motif, there are 481 amino acids (including oxBFP, AID and linkers), which is equivalent to *M*=44.

The probability that a ribosome locates at the i^{th} segment at time t is $p_i(t)$. We assumed the process is Markov and $p_i(t)$ satisfies a linear differential equation,

$$\frac{dp_i}{dt} = -kp_i + kp_{i-1} \tag{1}$$

for $1 < i \leq M$. The parameter *k* is the transition rate for ribosome between successive peptide segments. It is directly related to the translation elongation speed $v = 24k$ (each peptide segment contains 24 AA). It is necessary to point out that the translation between successive Suntag peptide is not a single step reaction, but rather many smaller steps. Therefore, Eq. 1 is only an approximation for the exact situation.

For the first segment, we have to take the translation initiation into account

$$\frac{dp_1}{dt} = -kp_1 + f(t) \tag{2}$$

where $f(t)$ is the initiation rate at time *t*. Here we assume the translation is at steady state and there is a constant initiation rate $f(t) = c$.

There are some implicit assumptions for the models given in Eq. 1. (a) The scFV-sfGFP binding to the nascent peptide is not rate-limiting and the binding on-rate is rapid compared to the imaging time resolution. (b) The dissociation rate of the scFV-sfGFP bound on epitope is slow compared with the recovery time. The assumption is validated by observing the slow recovery in the presence of translation inhibitor cycloheximide (CHX, 100 μg/mL). CHX stalls translation elongation and prohibits synthesis of new nascent peptides when administered at high concentration. (c) The newly synthesized protein diffuse away rapidly compared to the imaging time. (d) The different ribosomes translate independent from each other. This assumption is only valid if the ribosomes on mRNA are sparse.

The fluorescence at the translation site is

$$F(t) = \theta\left(\sum_{i=1}^{N} ip_i(t) + N\sum_{i=m+1}^{M} p_i(t)\right), \tag{3}$$

where θ is the effective brightness of a single epitope labeled by scFV-sfGFP. The mean value of the normalized fluorescence at steady state is

$$\frac{F_0}{N\theta} = \frac{c}{k}\left(M - \frac{1}{2}(N-1)\right), \tag{4}$$

where we have used the fact that $p_i = c/k$ at steady state. So the mean value of the translation intensity is directly proportional to the length of the ORF.

For FRAP experiment, the fluorescence at the translation site is bleached at *t*=0. The recovery in fluorescence comes from two sources: the first one is newly arrived ribosomes synthesizing *de novo* new proteins; the second one is the existing ribosomes which have not finished synthesizing the Suntag motif synthesizing the rest Suntag motif(See Figure 3K). We consider these two scenarios separately in the following.

For newly arrived ribosomes, the set of differential equation is solved with the initial conditions: $p_i(0) = 0$,

$$p_i(t; k, k_r) = \frac{c}{k}(1 - Q(i, kt)\ ), \tag{5}$$

for *i*<*n*, where $Q(a, x) = \Gamma(a, x)/\Gamma(a)$ is the regularized Gamma function $\Gamma(a, x) = \int_x^\infty t^{a-1} exp(-t) dt$. The fluorescence intensity due to the newly arrived ribosome is

$$F_{New}(t) = \theta\left(\sum_{i=1}^{N} i p_i(t) + N \sum_{i=N+1}^{M} p_i(t)\right), \tag{6}$$

For existing ribosomes, the fluorescence recovery is

$$F_{Ext}(t) = \sum_{i=1}^{N} \sum_{j>i}^{M} \theta_{i,j} p_i(0) p(j, t|i, 0), \tag{7}$$

where $\theta_{i,j}$ is the recovered intensity when the ribosome moved from peptide segment *i* to *j*:

$$\theta_{i,j} = \begin{cases} \theta(j - i), & for\ j < N, i < N \\ \theta(N - i) & for\ j > N, i < N\,. \\ 0 & for\ i \geq N \end{cases} \tag{8}$$

$p(j, t|i, 0)$ is the transition probability for the ribosome moved from *i* to *j*. Note for ribosomes that have translated the whole Suntag motif, there are no recovery. Solving the Eq.1 with the initial condition $p_l(0) = \delta_{i,l}$, we get,

$$p(j, \tau|i, 0) = \frac{(k\tau)^{j-i}}{(j-i)!} e^{-k\tau}. \tag{9}$$

The total recovered is the sum of the two scenarios,

$$F(t) = F_{New}(t) + F_{Ext}(t). \tag{10}$$

At steady state, there is no change in probability density $\frac{dp_i}{dt} = 0$, which means

$$p_i^0 = \frac{c}{k}. \tag{11}$$

The steady state fluorescence signal is by Eq. 4.

The normalized recovery curve is given by

$$f(t; k) = \frac{F(t)}{F_0}, \tag{12}$$

which only depends on one parameters: k. The initiation rate is eliminated during the normalization. The length of the gene (*M*) is a constant for a given reporter. The analytical solution is somewhat cumbersome. But it is only a finite sum of well-behaved function and can be calculated readily with a computer program

$$f(t; k) = \frac{2}{N(2M-N+1)}\Big(\sum_{i=1}^{N}\Big(i\big(1 - Q(i, kt)\big) + kt\ Q(N - i, kt) + (N - i)\big(Q(M + 1 - \tag{13}$$

$$i,kt) - Q(N+1-i,kt))\Big) + N\sum_{i=N+1}^{M}\Big((1-Q(i,kt))\Big)\Big).$$

In the case when the gene is extremely long ($M \gg N$), the solution can be simplified to a simple truncated straight line

$$f(t;k) = \left(\frac{kt}{M-\frac{N-1}{2}} - 1\right) H\left(1 - \frac{kt}{M-\frac{N-1}{2}}\right) + 1, \tag{14}$$

where $H(x)$ is the Heaviside step function (Fig. S4).

Derivation of the autocorrelation for translation

In neurons, assume that the mRNA exists in two different states, s_0 and s_1. The s_0 is a state where the mRNA is repressed from translation. Only in the state s_1, the mRNA can be translated. The two states interchange with rate

$$s_0 \underset{k_0}{\overset{k_1}{\leftrightarrows}} s_1, \tag{15}$$

which is essentially a random telegraph model. We assume that in state s_1 the translation follows similar dynamics as described in the previous section: there is a constant initiation rate *c* and the elongation rate of ribosome is a constant. In addition to this, we make another crucial hypothesis: the translation in subsequent translation active states are statistically independent. If we consider the translations happen in bursts, the implication of the hypothesis is that translation in different bursts is not correlated.

The average fluorescence at time *t* is

$$\langle F(t)\rangle = \sum_I \sum_s IP(I,s,t), \tag{16}$$

where *I* is the TLS intensity and $P(I,s,t)$ is the probability that the TLS has intensity *I* in state *s* at time t. Since the mRNA is not translating at state s_0,

$$\langle F(t)\rangle = \alpha \sum_I IP(I|s=1) = \alpha I_0, \tag{17}$$

where I_0 is the average intensity when the mRNA is in state s_1 and $\alpha = k_0/(k_1+k_0)$ is the steady state probability that the state is in state s_1.

The autocorrelation function for the TLS intensity is

$$\langle F(0)F(t)\rangle = \sum_I \sum_s I(t)I(0)P\big(I(t),s(t),I(0),s(0)\big), \tag{18}$$

where $P\big(I(t),s(t),I(0),s(0)\big)$ is the joint probability for translation status in state $s(0)$ and $s(t)$, with intensity $I(0)$ and $I(t)$, at time 0 and *t* respectively. The summations are over all possible intensities and states. With Bayes' theorem and the fact $I = 0$ when $s = 0$, we get

$$\langle F(0)F(t)\rangle = \sum_{I(t),I(0)} I(t)I(0)P(I(t)|s(t)=1,I(0),s(0)=1)P(s(t)=1|I(0),s(0) = 1)P(I(0)|s(0)=1)P(s(0)=1), \tag{19}$$

The transition probability for random telegraph model is given by (*42*):

$$P(s(t)=1|s(0)=1) = \alpha + (1-\alpha)e^{-(k_0+k_1)t} \tag{20}$$

There are two scenarios for $s(t)=1$ and $s(0)=1$:

Case I: $s(t)=1$ is in the same burst as $s(0)=1$,

$$P(s(t)=1, in\ the\ same\ burst|s(0)=1) = e^{-k_1 t}, \tag{21}$$

in which case $I(t)$ and $I(0)$ are correlated:

$$\begin{aligned} &P(I(t)|s(t)=1, I(0), s(0)=1)P\big(s(t)=1|s(0)=1, I(0)\big) \\ &\quad = P(I(t)|I(0), s(t)=1, s(0)=1\ in\ the\ same\ burst)e^{-k_1 t}. \end{aligned} \tag{22}$$

Case II: $s(t)=1$ is in another burst,

$$P(s(t)=1, in\ another\ burst|s(0)=1) = \alpha + (1-\alpha)e^{-(k_0+k_1)t} - e^{-k_1 t}, \tag{23}$$

in which case $I(t)$ and $I(0)$ are statistically independent:

$$\begin{aligned} &P(I(t)|s(t)=1, I(0), s(0)=1)P(s(t)=1|I(0), s(0)=1) \\ &\quad = \big(\alpha + (1-\alpha)e^{-(k_0+k_1)t} - e^{-k_1 t}\big)P(I(t)|s(t)=1). \end{aligned} \tag{24}$$

Taken together,

$$\begin{aligned} &\langle F(0)F(t)\rangle \\ &= \alpha e^{-k_1 t} \sum_{I(t),I(0)} I(t)I(0)P(I(t)|I(0), s(t), s(0)\ are\ in\ the\ same\ burst)P(I(0)|s(0)=1) \\ &+ \alpha\big(\alpha + (1-\alpha)e^{-(k_0+k_1)t} - e^{-k_1 t}\big) \sum_{I(t),I(0)} I(t)I(0)P(I(t)|s(t)=1\,)P(I(0)|s(0)=1). \end{aligned} \tag{25}$$

In the second term, the summation can be factorized since $I(t)$ and $I(0)$ are statistically independent. The first term is just the definition of the autocorrelation for constitutive translation,

$$\langle F(0)F(t)\rangle = \alpha e^{-k_1 t}\langle I(0)I(t)\rangle_0 + \alpha\big(\alpha + (1-\alpha)e^{-(k_0+k_1)t} - e^{-k_1 t}\big){I_0}^2 \tag{26}$$

where $\langle I(0)I(t)\rangle_0$ and I_0 are the autocorrelation and average fluorescence intensity respectively, when mRNAs are constitutively translated. The autocorrelation function is defined as

$$G(t) = \frac{\langle F(0)F(t)\rangle - \langle F(0)\rangle^2}{\langle F(0)\rangle^2} = \frac{e^{-k_1 t}g(t) + (1-\alpha)e^{-(k_0+k_1)t}}{\alpha}, \tag{27}$$

where $g(t) = (\langle I(0)I(t)\rangle_0 - \langle I\rangle_0^2)/\langle I\rangle_0^2$ is the autocorrelation function when the mRNA is constitutively translated. For the special case that there is no fluctuation in intensity $g(t)=0$, the autocorrelation function is reduced to that of a pure random telegraph model:

$$G(t) = \frac{(1-\alpha)}{\alpha}e^{-(k_0+k_1)t}. \tag{28}$$

The amplitude of the autocorrelation function is

$$G(0) = \frac{g(0) + (1-\alpha)}{\alpha}. \tag{29}$$

Since $\alpha < 1$, the $G(0)$ is increased due to the extra fluctuation due to the translation is turned on and off.

So far, the derivation is general and holds no assumption for the translation dynamics in each burst. If we further assume that the translation in each burst is with constant initiation rate *c* and elongation rate *k*, the autocorrelation function $g(t)$ can be derived analytically similar to the transcription dynamics (*5*). In the case that the Suntag is placed at the N-terminal of the reporter, the autocorrelation function can be approximated as

$$G(t;c,T) = \frac{T-t}{cT^2}H(T-t), \tag{30}$$

where $H(x)$ is the Heaviside step function. The parameter *c* is the translation initiation rate. The residence time $T = M/k$. In practice, *T* also includes the release time from the translation sites. Therefore, the final equations we used to fit the equation for bursting translation is

$$G(t;c,T,k_0,k_1) = \frac{\frac{T-t}{cT^2}H(T-t)e^{-k_1 t} + (1-\alpha)e^{-(k_0+k_1)t}}{\alpha}. \tag{31}$$

3. Supplemental Figure Legends

Fig. S1. IAA reduced the level of protein containing auxin induced degron (AID).
U2OS cells stably expressing OsTIR1, scFV-sfGFP and flag-SINAPS were incubated with 500μM of IAA overnight. The level of flag-SINAPS was reduced to undetectable by western blot. The αGFP primary antibody detected oxBFP in flag-SINAPS and sfGFP in scFV-sfGFP respectively. The scFV-sfGFP was used as a loading control.

Fig. S2. smFISH & IF analysis of SINAPS reporter in fixed cells.

U2OS cells stably expressing OsTIR1, scFV-sfGFP and flag-SINAPS were treated with 100μg/mL puromycin for 10 minutes (A-B). After fixation, FISH & IF were performed. (A) There were only dim single protein spots (green). Bright translation sites were not detectable any more. A portion of the cell was magnified in (B). In another set of experiments (C-E), after treatment with 100μg/mL puromycin, the cells were washed and incubated in the normal medium for 20 minutes before fixing for FISH & IF experiments. Bright translation sites reappeared and colocalized with mRNA. The number of NAPs at TLS was comparable to the steady state condition. (B,D) Yellow arrow head: translation sites; white arrow head: single flag-SINAPS protein; white arrow: non translating mRNAs. Scale Bars: A, C: 5μm, B, D: 2 μm. (F) The number of NAPs when cells were treated with 2μg/mL of CHX. More NAPs accumulated on mRNAs: the average number of NAPs was 5 with higher population containing more NAPs. (G) Different constructs to vary the length of the coding region. Between Suntag and AID, the insertion is: 1, nothing; 2: oxBFP (239aa); 3: Fluc: Firefly Luciferase (550aa); 4: Firefly Luciferase + oxBFP (796aa).

Fig. S3. CytERM-SINAPS proteins were localized on the ER

U2OS cells stably expressing OsTIR1, scFV-sfGFP were transiently transfected with CytERM-SINAPS. (A-B): a high expression cell. (C-D): a low expression cells. The boxes in A, C were shown in B, D. Scale bars: A,C: 5 μm ; B,D: 2 μm. (E) Single CytERM-SINAPS proteins from low expression cells were tracked (Movie S4). The diffusion coefficient of a single protein was significantly larger than that of the translation sites.

Fig. S4. Theoretical modeling of fluorescence recovery after photobleaching

(A) The schematic of Monte Carlo simulation algorithm. A ribosome initiates the translation randomly with a rate *c* (1/s). Then it moves from one state (a Suntag peptide) to the next with a probability proportional to a rate *k*. The fluorescence of a ribosome depends on its position (given at the bottom panel). The total fluorescence is calculated by sum of all ribosomes on the mRNA at that time. The simulation first runs to equilibrium. For bleaching, the fluorescence is set to 0 at time 0. The simulation continues as usual and the recovered fluorescence is sampled every 10 seconds just as in experiments. (B) An example trace of Monte Carlo simulation. The parameter used in the simulation: translation initiation rate *c*=0.025/s (or 1.5/min), elongation rate *k*=0.25/s (or 6 AA/s), the number of Suntag epitopes N=24, the total length of the reporter in units of Suntag epitope size M=44, the time step used in the simulation $dt = \frac{0.001}{c}$. (C) Comparison between the Monte Carlo simulated recovery curve (symbol, averaged over 10000 simulations) with the theoretical prediction (line) according to Eq. 13. The theoretical prediction involves only one parameter: the elongation speed. The theory matches the simulation well. (D) Theoretical prediction of FRAP curves for different reporter length. The length of reporter is given in units of Suntag epitope size. The longer the mRNA, the longer it takes to recover. (E) Comparison between the exact theory (Eq. 13) and the approximation with a truncated linear recovery curve (Eq. 14) for *N*=24, *M*=44.

Fig. S5. FRAP of TLS with different ORF lengths

We made CytERM-SINAPS constructs with different length by inserting various protein sequence between Suntag motif and AID (A: M=34, B: M=44, C: M=67 in units of Suntag epitope size, Material and Methods). The lengths of the coding region after the Suntag motif were shown in the figure. The constructs were transiently transfected into U2OS cells stably expressing OsTIR1 and scFV-sfGFP. FRAP experiments were performed on single TLS. Fitting the FRAP theory to the experimental data yielded the elongation rate: (A), $v = 5.6 \pm 1.4 AA/s$; (B), $v = 4.7 \pm 0.6 AA/s$; (C), $v = 5.0 \pm 1.1 AA/s$, all within the experimental uncertainty. So a single parameter was able to describe all the FRAP data. The figure (B) is the same as Fig. 4E in the main text, and is shown here for comparison.

Fig. S6. FISH & IF of neurons and glial cells

(A) The FISH & IF image of the neuron shown in Fig. 5A-C. The selected dendrite was marked. (B) The histogram of the number of NAPs at TLS in dendrite. (C) The FISH & IF image of a glial cell. The box was shown in (D), Left (red): FISH of mRNA; middle (green): IF of Suntag; right: merge. Scale bars: 5μm. (E) The histogram of the number of NAPs at translation sites in Glia.

Fig. S7. Puromycin treatment of neurons

The hippocampal neurons infected with flag-SINAPS and OsTIR1-IRES-scFV-sfGFP were treated with 100 μg/mL puromycin (A-C). The translations sites before treatments (A) disappeared completely 2 minutes after treatment (B) in the same neuron. The number of translation sites was quantified in (C).

4. Supplemental Movies

Movie S1: Translation sites and mRNAs of flag-SINAPS were moving together
U2OS Cell (Fig. 2A) stably expressing scFV-sfGFP, OsTIR1, stdMCP-Halo and flag-SINAPS was streamed at 50ms for 200 frames. Green: scFV-sfGFP, Red: stdMCP-Halotag-JF549. Scale Bar: 5 μm

Movie S2: A selected portion of the cell shown in Movie S1 and Figs. 2B-D
Left: mRNA, middle: TLS and free protein, right: merge. Scale Bar: 2 μm. The red circles were tracked mRNA. The green square was tracked TLS. In the movie, we showed the tracks of one translating mRNA and one untranslating mRNA.

Movie S3: Translation sites disappeared in the presence of puromycin
U2OS Cell stably expressing scFV-sfGFP, OsTIR1, stdMCP-Halo and flag-SINAPS was streamed at 50ms for 200 frames in the presence of 100μg/mL puromycin. There were no bright green TLS moving together with mRNAs. Green: scFV-sfGFP, Red: stdMCP-Halotag-JF549. Scale Bar: 5μm.

Movie S4: Single CytERM-SINAPS proteins could be tracked
U2OS Cell (Fig. S3) stably expressing scFV-sfGFP, OsTIR1 and CytERM-SINAPS was streamed at 50ms for 60 frames. Single CytERM-SINAPS protein (green circle) on the ER membrane could be tracked. The translation site (Green square) was confined and much brighter. Scale bar: 2 μm.

Movie S5: Comparing the diffusion of flag-SINAPS and CytERM-SINAPS mRNAs
U2OS cells stably expressing stdMCP-stdGFP were transiently transfected with flag-SINAPS (left panel) or CytERM-SINAPS (middle and right panels) constructs. All mRNAs were labeled with stdMCP-stdGFP (*22*). Most of cytoplasmic flag-SINAPS were freely diffusing (left). In contrast, CytERM-SINAPS mRNAs were mostly confined (middle). However, when treated with puromycin, most CytERM-SINAPS mRNAs became freely diffusing (right), very similar to the flag-SINAPS mRNAs (left). Note the mRNAs were labeled by stdMCP-stdGFP and scFV-sfGFP was not expressed in the cells. The white ovals were draw to isolate nuclei regions. The yellow boxes drawn in each panel were arbitrary regions in the cytoplasm and meant to focus the attention. Scale bar: 5μm.

Movie S6: CytERM-SINAPS TLS were confined, while non-translating mRNAs were freely diffusion
U2OS Cell (Fig. 3) stably expressing scFV-sfGFP, OsTIR1, stdMCP-Halo and CytERM-SINAPS was streamed at 50ms for 200 frames. Green: scFV-sfGFP, Red: stdMCP-Halotag-JF549. Scale Bar: 5 μm

Movie S7: A selected portion of the cell shown in Movie S6 and Figs. 3D-F
Left: mRNA, middle: TLS and free proteins, right: merge. Scale Bar 2 μm. The red circles were tracked mRNAs. The green square was a tracked TLS. In the movie, we showed the tracks of one translating mRNA and one untranslating mRNA. The translating mRNA was confined and the untranslating mRNA was freely diffusing.

Movie S8: CytERM-SINAPS TLS disappeared and mRNAs freely diffused in the presence puromycin
U2OS Cell stably expressing scFV-sfGFP, OsTIR1, stdMCP-Halo and CytERM-SINAPS was streamed at 50ms for 200 frames in the presence of 100μg/mL puromycin. There were no bright green translation

sites moving together with mRNAs. In addition, all mRNAs were freely diffusing instead of confined. Green: scFV-sfGFP, Red: stdMCP-Halotag-JF549. Scale Bar: 2μm.

Movie S9: FRAP of a single TLS: The overview of the whole cell
After two pre-bleaching images, a single selected translation site was bleached before frame 3 in U2OS cells stably expressing scFV-sfGFP, OsTIR1 and CytERM-SINAPS. The fluorescence recovery was monitored with time lapse imaging every 10s. The images were max-projection of z-stacks. Top: the FRAP movie with tracked TLS; bottom: the fluorescence intensity of the bleached TLS. Scale bar: 5 μm.

Movie S10: FRAP of single TLSs: comparison between different conditions
Single translation sites were bleached in U2OS cells stably expressing scFV-sfGFP, OsTIR1 and CytERM-SINAPS. Left: control; middle: non-bleached; right: bleached in the presence of CHX. Scale bar: 2μm.

Movie S11: Flag-SINAPS in hippocampal neuron: overview of TLS in the neuron.
Primary hippocampal neurons were infected with OsTIR1-IRES-scFV-sfGFP and flag-SINAPS. The neuron was imaged with time-lapse movie every one minute. The ROI was straightened and showed in Movie S12 and analyzed in Fig. 6A-C. Scale bar: 5 μm

Movie S12: Tracking of TLS in neuron
Analysis of the TLSs in selected ROI shown in Movie S11. Top: original movie; middle: inverted and the TLS tracked; bottom: the integrated intensities of tracked translation sites in the middle panel. Scale bar: 5 μm

Movie S13: An example of TLS scanning along the dendrite
Primary hippocampal neurons were infected with OsTIR1-IRES-scFV-sfGFP and flag-SINAPS. Top: original movie; middle: inverted and the TLS tracked; bottom: the integrated intensities of tracked translation sites in the middle panel. Scale bar: 5 μm

Movie S14: Constitutive translating mRNAs in neuron
A constitutively translating mRNA in primary hippocampal neurons infected with OsTIR1-IRES-scFV-sfGFP and flag-SINAPS. Top: original movie; middle: inverted and the TLS tracked; bottom: the integrated intensity of tracked translation site in the middle panel. Scale bar: 5 μm

Fig. S1

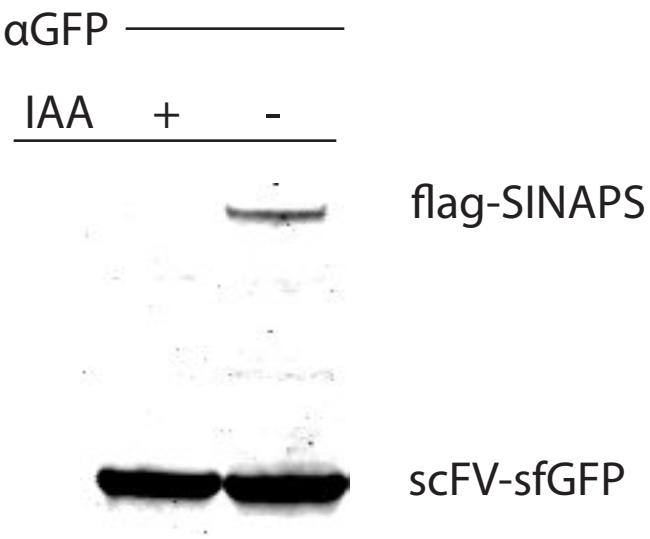

Fig. S2

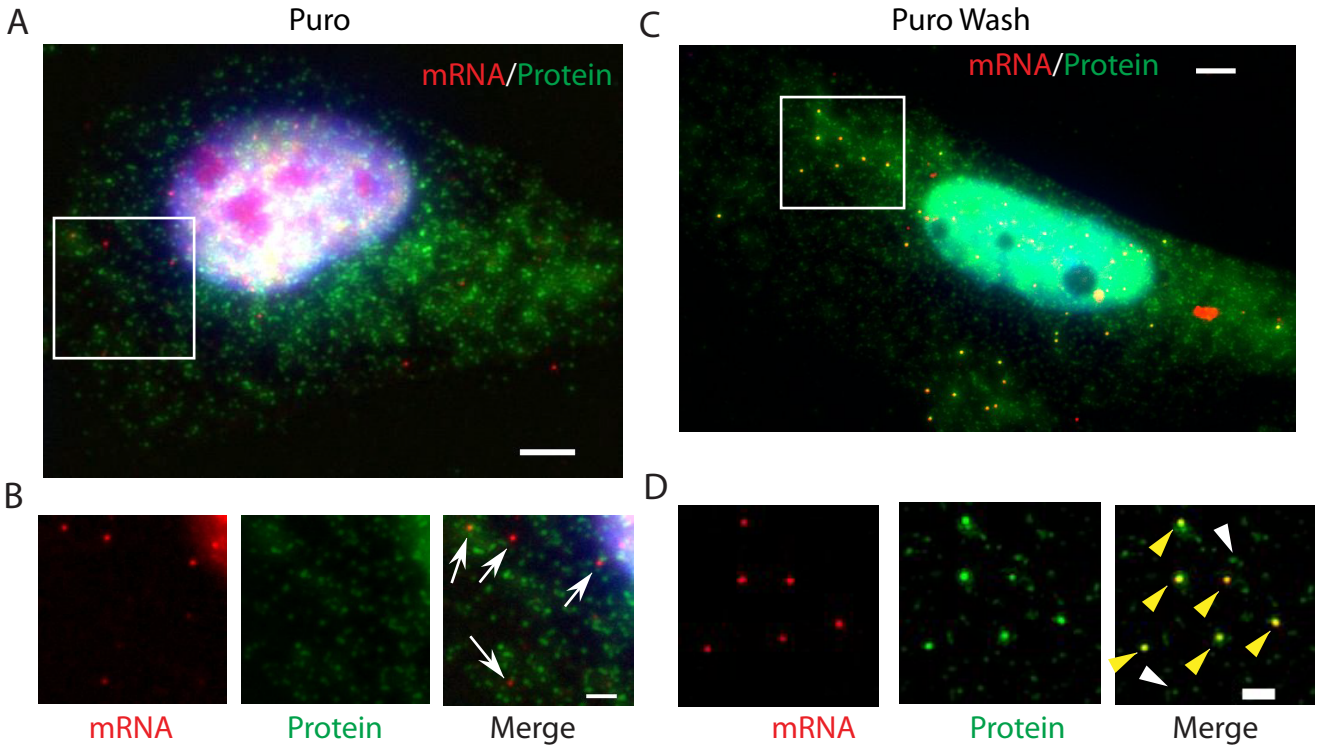
A
Puro
mRNA/Protein
C
Puro Wash
mRNA/Protein
B
mRNA
Protein
Merge
D
mRNA
Protein
Merge

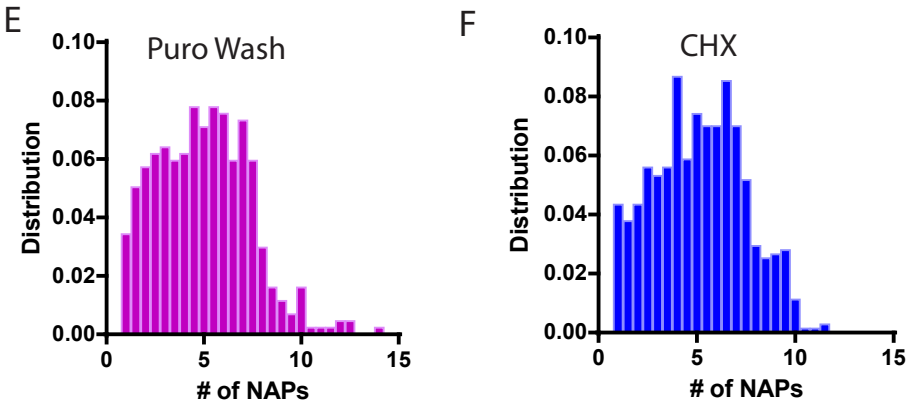
E
Puro Wash
Distribution
0.10
0.08
0.06
0.04
0.02
0.00
0
5
10
15
# of NAPs
F
CHX
Distribution
0.10
0.08
0.06
0.04
0.02
0.00
0
5
10
15
# of NAPs

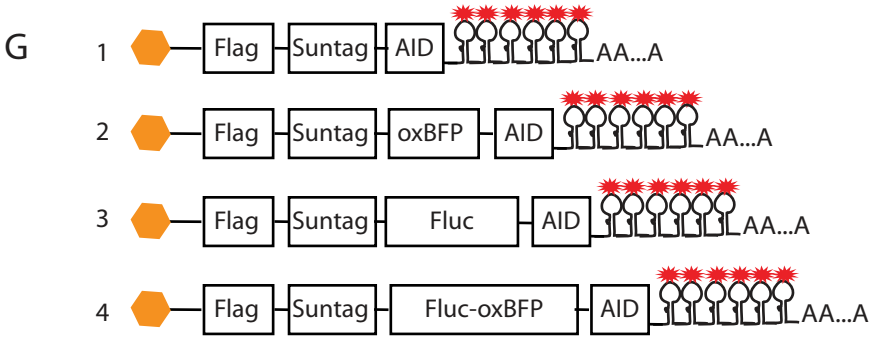
G
1
Flag
Suntag
AID
AA...A
2
Flag
Suntag
oxBFP
AID
AA...A
3
Flag
Suntag
Fluc
AID
AA...A
4
Flag
Suntag
Fluc-oxBFP
AID
AA...A

Fig. S3

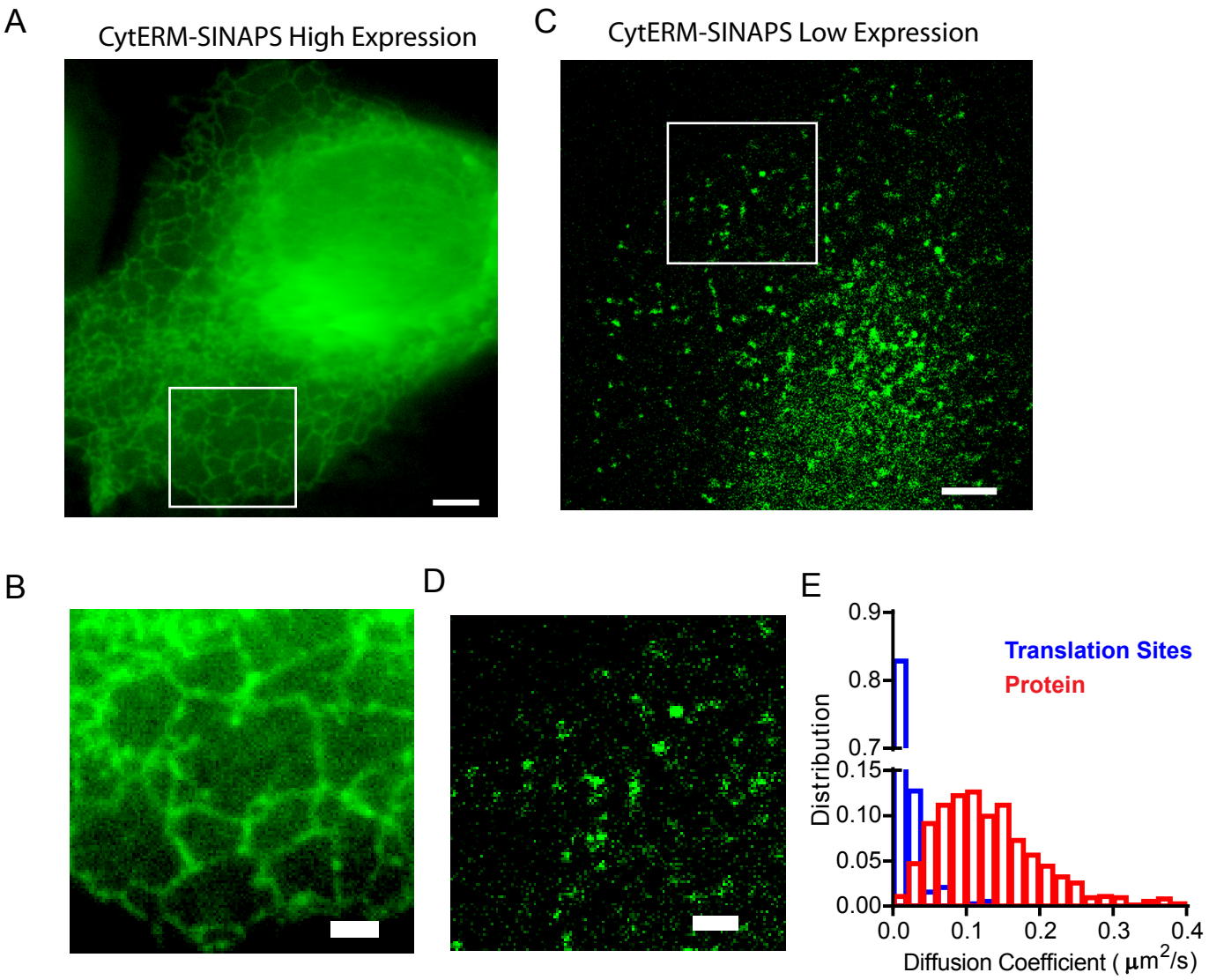
A
CytERM-SINAPS High Expression
C
CytERM-SINAPS Low Expression
B
D
E
Translation Sites
Protein
Distribution
0.9
0.8
0.7
0.15
0.10
0.05
0.00
0.0
0.1
0.2
0.3
0.4
Diffusion Coefficient (μm2/s)

Fig. S4

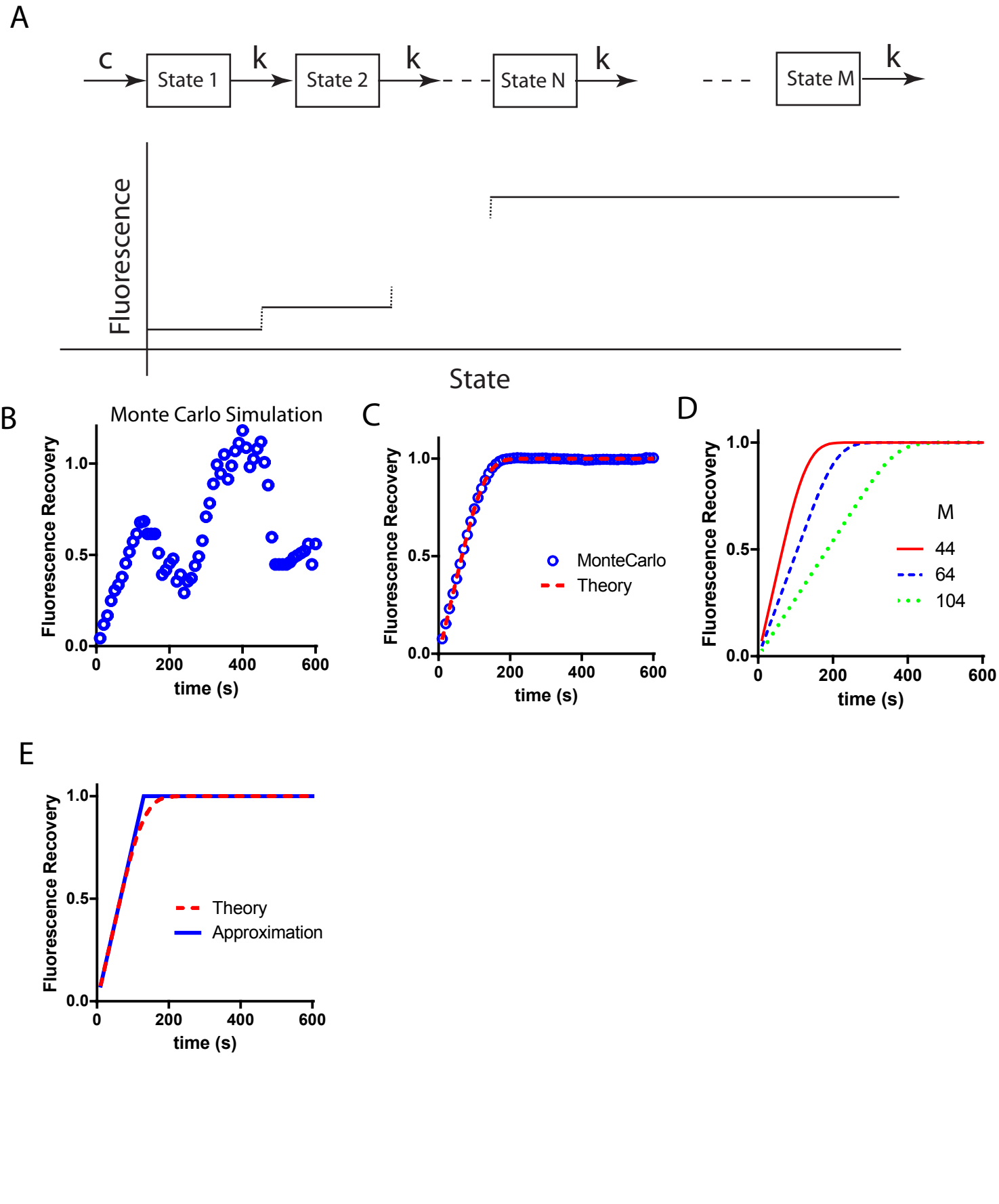
A
c
State 1
k
State 2
k
State N
k
State M
k
Fluorescence
State
B
Monte Carlo Simulation
Fluorescence Recovery
1.0
0.5
0.0
0
200
400
600
time (s)
C
Fluorescence Recovery
MonteCarlo
Theory
time (s)
D
Fluorescence Recovery
M
44
64
104
time (s)
E
Fluorescence Recovery
Theory
Approximation
time (s)

Fig. S5

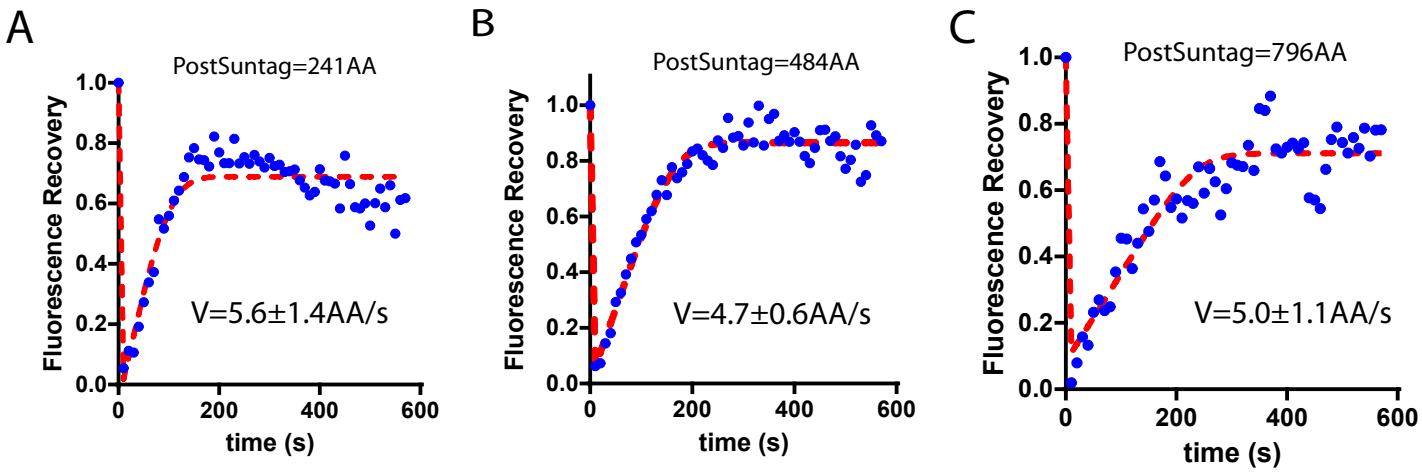
A
PostSuntag=241AA
Fluorescence Recovery
1.0
0.8
0.6
0.4
0.2
0.0
0
200
400
600
time (s)
V=5.6±1.4AA/s
B
PostSuntag=484AA
Fluorescence Recovery
1.0
0.8
0.6
0.4
0.2
0.0
0
200
400
600
time (s)
V=4.7±0.6AA/s
C
PostSuntag=796AA
Fluorescence Recovery
1.0
0.8
0.6
0.4
0.2
0.0
0
200
400
600
time (s)
V=5.0±1.1AA/s

Fig. S6

A

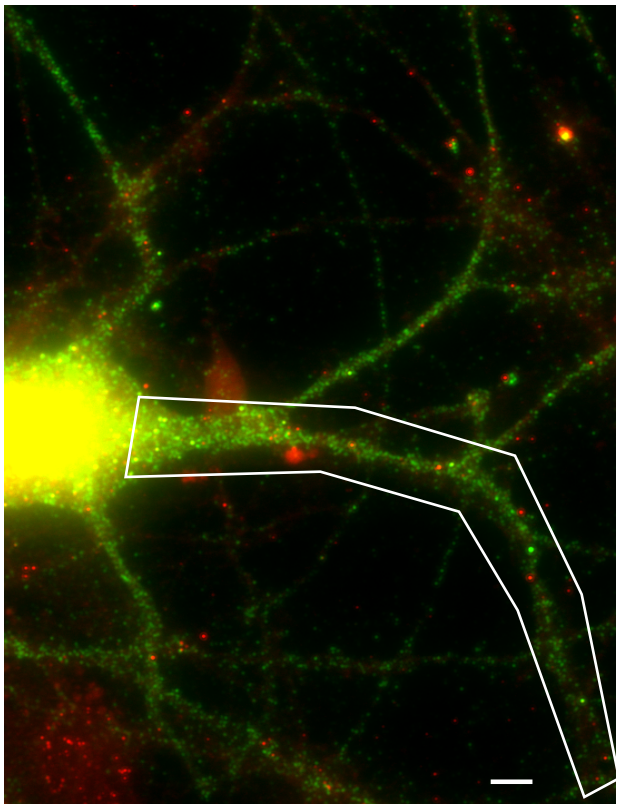

mRNA/Protein

B

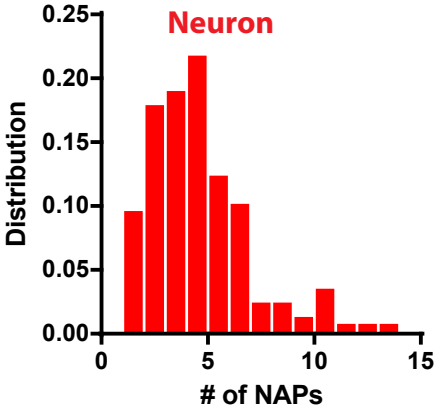

C

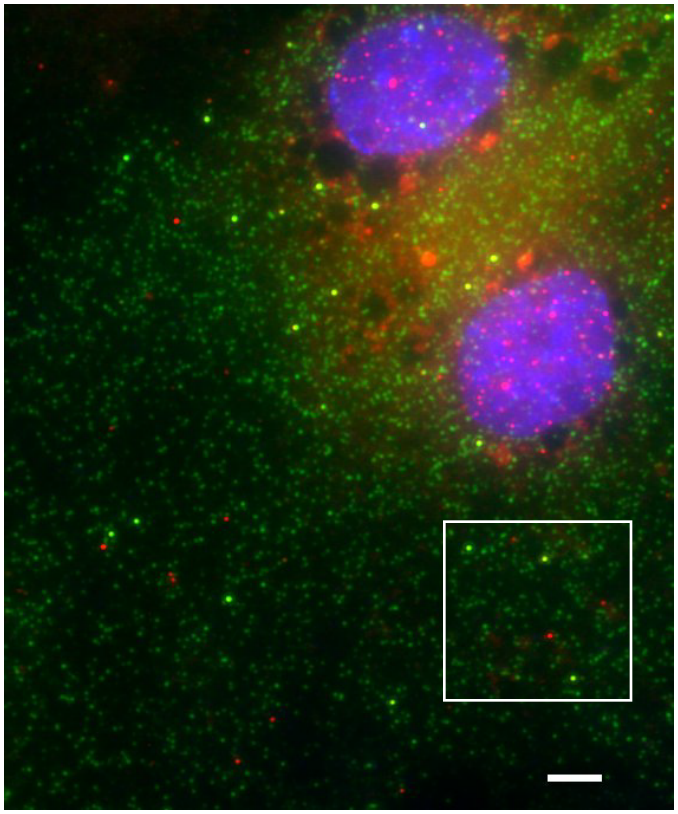

mRNA/Protein

D

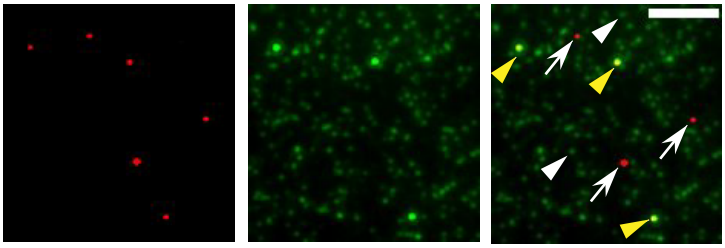

mRNA Protein Merge

E

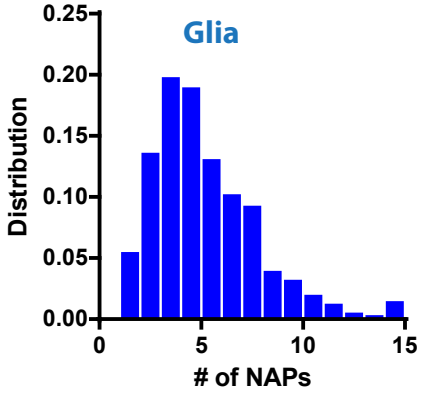

Fig. S7

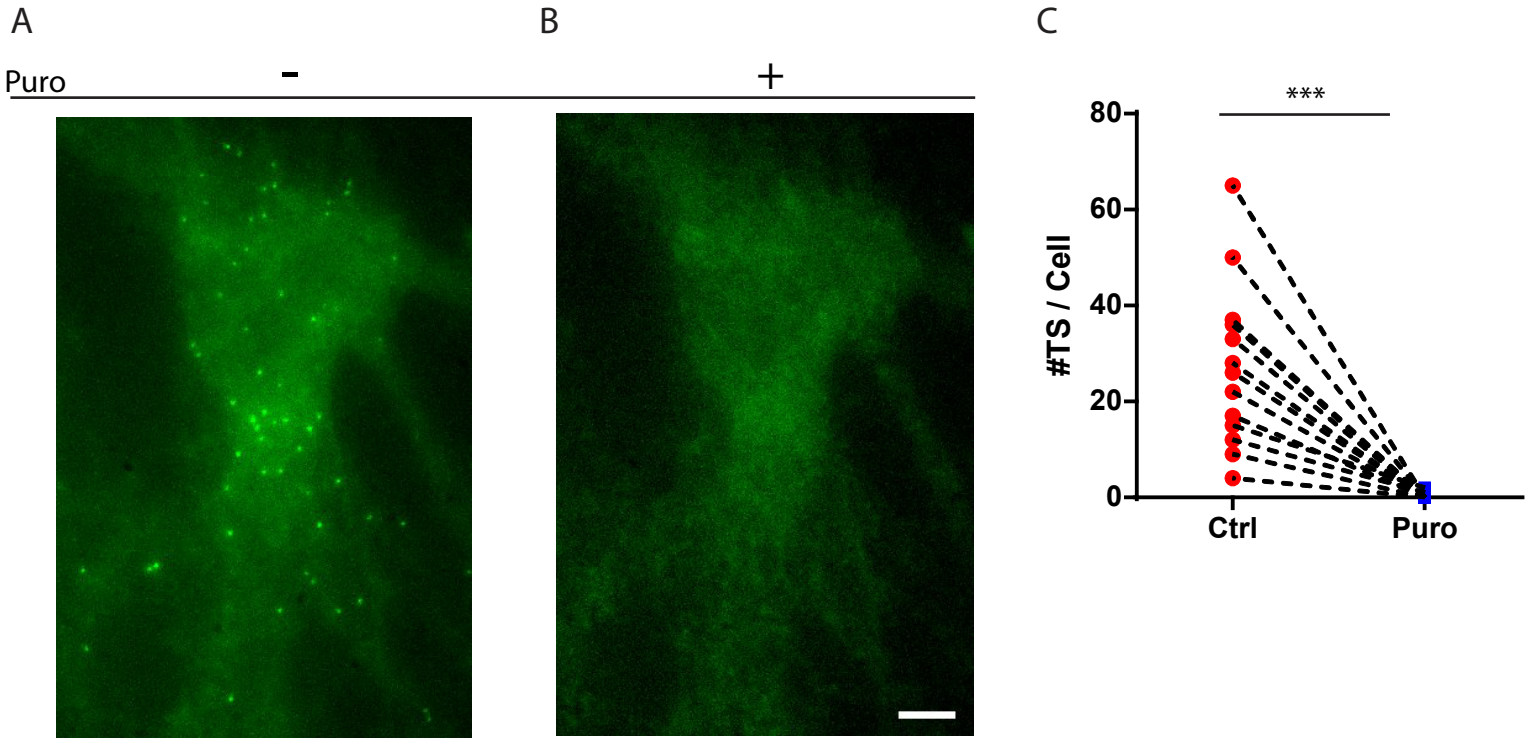

References and Notes

1. B. Schwanhäusser, D. Busse, N. Li, G. Dittmar, J. Schuchhardt, J. Wolf, W. Chen, M. Selbach, Global quantification of mammalian gene expression control. *Nature* **473**, 337–342 (2011). Medline doi:10.1038/nature10098

2. N. Sonenberg, A. G. Hinnebusch, Regulation of translation initiation in eukaryotes: Mechanisms and biological targets. *Cell* **136**, 731–745 (2009). Medline doi:10.1016/j.cell.2009.01.042

3. C. E. Holt, E. M. Schuman, The central dogma decentralized: New perspectives on RNA function and local translation in neurons. *Neuron* **80**, 648–657 (2013). Medline doi:10.1016/j.neuron.2013.10.036

4. A. R. Buxbaum, G. Haimovich, R. H. Singer, In the right place at the right time: Visualizing and understanding mRNA localization. *Nat. Rev. Mol. Cell Biol.* **16**, 95–109 (2015). Medline doi:10.1038/nrm3918

5. D. R. Larson, D. Zenklusen, B. Wu, J. A. Chao, R. H. Singer, Real-time observation of transcription initiation and elongation on an endogenous yeast gene. *Science* **332**, 475–478 (2011). Medline doi:10.1126/science.1202142

6. N. T. Ingolia, S. Ghaemmaghami, J. R. Newman, J. S. Weissman, Genome-wide analysis in vivo of translation with nucleotide resolution using ribosome profiling. *Science* **324**, 218–223 (2009). Medline doi:10.1126/science.1168978

7. C. H. Jan, C. C. Williams, J. S. Weissman, Principles of ER cotranslational translocation revealed by proximity-specific ribosome profiling. *Science* **346**, 1257521 (2014). Medline doi:10.1126/science.1257521

8. B. Wu, A. R. Buxbaum, Z. B. Katz, Y. J. Yoon, R. H. Singer, Quantifying Protein-mRNA Interactions in Single Live Cells. *Cell* **162**, 211–220 (2015). Medline doi:10.1016/j.cell.2015.05.054

9. D. C. Dieterich, J. J. Hodas, G. Gouzer, I. Y. Shadrin, J. T. Ngo, A. Triller, D. A. Tirrell, E. M. Schuman, In situ visualization and dynamics of newly synthesized proteins in rat hippocampal neurons. *Nat. Neurosci.* **13**, 897–905 (2010). Medline doi:10.1038/nn.2580

10. S. R. Starck, H. M. Green, J. Alberola-Ila, R. W. Roberts, A general approach to detect protein expression in vivo using fluorescent puromycin conjugates. *Chem. Biol.* **11**, 999–1008 (2004). Medline doi:10.1016/j.chembiol.2004.05.011

11. G. Aakalu, W. B. Smith, N. Nguyen, C. Jiang, E. M. Schuman, Dynamic visualization of local protein synthesis in hippocampal neurons. *Neuron* **30**, 489–502 (2001). Medline doi:10.1016/S0896-6273(01)00295-1

12. D. O. Wang, S. M. Kim, Y. Zhao, H. Hwang, S. K. Miura, W. S. Sossin, K. C. Martin, Synapse- and stimulus-specific local translation during long-term neuronal plasticity. *Science* **324**, 1536–1540 (2009). Medline doi:10.1126/science.1173205

13. M. T. Butko, J. Yang, Y. Geng, H. J. Kim, N. L. Jeon, X. Shu, M. R. Mackey, M. H. Ellisman, R. Y. Tsien, M. Z. Lin, Fluorescent and photo-oxidizing TimeSTAMP tags

track protein fates in light and electron microscopy. *Nat. Neurosci.* **15**, 1742–1751 (2012). Medline doi:10.1038/nn.3246

14. Y. Taniguchi, P. J. Choi, G. W. Li, H. Chen, M. Babu, J. Hearn, A. Emili, X. S. Xie, Quantifying E. coli proteome and transcriptome with single-molecule sensitivity in single cells. *Science* **329**, 533–538 (2010). Medline doi:10.1126/science.1188308

15. J. M. Halstead, T. Lionnet, J. H. Wilbertz, F. Wippich, A. Ephrussi, R. H. Singer, J. A. Chao, An RNA biosensor for imaging the first round of translation from single cells to living animals. *Science* **347**, 1367–1671 (2015). Medline doi:10.1126/science.aaa3380

16. M. E. Tanenbaum, L. A. Gilbert, L. S. Qi, J. S. Weissman, R. D. Vale, A protein-tagging system for signal amplification in gene expression and fluorescence imaging. *Cell* **159**, 635–646 (2014). Medline doi:10.1016/j.cell.2014.09.039

17. J. D. Pédelacq, S. Cabantous, T. Tran, T. C. Terwilliger, G. S. Waldo, Engineering and characterization of a superfolder green fluorescent protein. *Nat. Biotechnol.* **24**, 79–88 (2006). Medline doi:10.1038/nbt1172

18. E. Bertrand, P. Chartrand, M. Schaefer, S. M. Shenoy, R. H. Singer, R. M. Long, Localization of ASH1 mRNA particles in living yeast. *Mol. Cell* **2**, 437–445 (1998). Medline doi:10.1016/S1097-2765(00)80143-4

19. A. J. Holland, D. Fachinetti, J. S. Han, D. W. Cleveland, Inducible, reversible system for the rapid and complete degradation of proteins in mammalian cells. *Proc. Natl. Acad. Sci. U.S.A.* **109**, E3350–E3357 (2012). Medline doi:10.1073/pnas.1216880109

20. K. Nishimura, T. Fukagawa, H. Takisawa, T. Kakimoto, M. Kanemaki, An auxin-based degron system for the rapid depletion of proteins in nonplant cells. *Nat. Methods* **6**, 917–922 (2009). Medline doi:10.1038/nmeth.1401

21. L. M. Costantini, M. Fossati, M. Francolini, E. L. Snapp, Assessing the tendency of fluorescent proteins to oligomerize under physiologic conditions. *Traffic* **13**, 643–649 (2012). Medline doi:10.1111/j.1600-0854.2012.01336.x

22. B. Wu, V. Miskolci, H. Sato, E. Tutucci, C. A. Kenworthy, S. K. Donnelly, Y. J. Yoon, D. Cox, R. H. Singer, L. Hodgson, Synonymous modification results in high-fidelity gene expression of repetitive protein and nucleotide sequences. *Genes Dev.* **29**, 876–886 (2015). Medline doi:10.1101/gad.259358.115

23. Material and methods are available as supplementary material on *Science* Online.

24. G. V. Los, L. P. Encell, M. G. McDougall, D. D. Hartzell, N. Karassina, C. Zimprich, M. G. Wood, R. Learish, R. F. Ohana, M. Urh, D. Simpson, J. Mendez, K. Zimmerman, P. Otto, G. Vidugiris, J. Zhu, A. Darzins, D. H. Klaubert, R. F. Bulleit, K. V. Wood, HaloTag: A novel protein labeling technology for cell imaging and protein analysis. *ACS Chem. Biol.* **3**, 373–382 (2008). Medline doi:10.1021/cb800025k

25. J. B. Grimm, B. P. English, J. Chen, J. P. Slaughter, Z. Zhang, A. Revyakin, R. Patel, J. J. Macklin, D. Normanno, R. H. Singer, T. Lionnet, L. D. Lavis, A general method to improve fluorophores for live-cell and single-molecule microscopy. *Nat. Methods* **12**, 244–250, 3, 250 (2015). Medline doi:10.1038/nmeth.3256

26. B. Wu, J. A. Chao, R. H. Singer, Fluorescence fluctuation spectroscopy enables quantitative imaging of single mRNAs in living cells. *Biophys. J.* **102**, 2936–2944 (2012). Medline doi:10.1016/j.bpj.2012.05.017

27. D. Grünwald, R. H. Singer, In vivo imaging of labelled endogenous β-actin mRNA during nucleocytoplasmic transport. *Nature* **467**, 604–607 (2010). Medline doi:10.1038/nature09438

28. T. Lionnet, K. Czaplinski, X. Darzacq, Y. Shav-Tal, A. L. Wells, J. A. Chao, H. Y. Park, V. de Turris, M. Lopez-Jones, R. H. Singer, A transgenic mouse for in vivo detection of endogenous labeled mRNA. *Nat. Methods* **8**, 165–170 (2011). Medline doi:10.1038/nmeth.1551

29. K. Jaqaman, D. Loerke, M. Mettlen, H. Kuwata, S. Grinstein, S. L. Schmid, G. Danuser, Robust single-particle tracking in live-cell time-lapse sequences. *Nat. Methods* **5**, 695–702 (2008). Medline doi:10.1038/nmeth.1237

30. T. A. Rapoport, Protein translocation across the eukaryotic endoplasmic reticulum and bacterial plasma membranes. *Nature* **450**, 663–669 (2007). Medline doi:10.1038/nature06384

31. N. T. Ingolia, L. F. Lareau, J. S. Weissman, Ribosome profiling of mouse embryonic stem cells reveals the complexity and dynamics of mammalian proteomes. *Cell* **147**, 789–802 (2011). Medline doi:10.1016/j.cell.2011.10.002

32. H. Jung, C. G. Gkogkas, N. Sonenberg, C. E. Holt, Remote control of gene function by local translation. *Cell* **157**, 26–40 (2014). Medline doi:10.1016/j.cell.2014.03.005

33. A. R. Buxbaum, B. Wu, R. H. Singer, Single β-actin mRNA detection in neurons reveals a mechanism for regulating its translatability. *Science* **343**, 419–422 (2014). Medline doi:10.1126/science.1242939

34. M. Doyle, M. A. Kiebler, Mechanisms of dendritic mRNA transport and its role in synaptic tagging. *EMBO J.* **30**, 3540–3552 (2011). Medline doi:10.1038/emboj.2011.278

35. A. Wörn, A. Auf der Maur, D. Escher, A. Honegger, A. Barberis, A. Plückthun, Correlation between in vitro stability and in vivo performance of anti-GCN4 intrabodies as cytoplasmic inhibitors. *J. Biol. Chem.* **275**, 2795–2803 (2000). Medline doi:10.1074/jbc.275.4.2795

36. C. H. Jan, C. C. Williams, J. S. Weissman, Response to Comment on "Principles of ER cotranslational translocation revealed by proximity-specific ribosome profiling". *Science* **348**, 1217 (2015). Medline doi:10.1126/science.aaa8299

37. D. W. Reid, C. V. Nicchitta, Diversity and selectivity in mRNA translation on the endoplasmic reticulum. *Nat. Rev. Mol. Cell Biol.* **16**, 221–231 (2015). Medline

38. D. W. Reid, C. V. Nicchitta, Comment on "Principles of ER cotranslational translocation revealed by proximity-specific ribosome profiling". *Science* **348**, 1217 (2015). Medline doi:10.1126/science.aaa7257

39. T. Morisaki *et al*., *Science* (2016). 10.1126/science.aaf0899

40. G. Mostoslavsky, A. J. Fabian, S. Rooney, F. W. Alt, R. C. Mulligan, Complete correction of murine Artemis immunodeficiency by lentiviral vector-mediated gene transfer. *Proc. Natl. Acad. Sci. U.S.A.* **103**, 16406–16411 (2006). Medline doi:10.1073/pnas.0608130103

41. F. Mueller, A. Senecal, K. Tantale, H. Marie-Nelly, N. Ly, O. Collin, E. Basyuk, E. Bertrand, X. Darzacq, C. Zimmer, FISH-quant: Automatic counting of transcripts in 3D FISH images. *Nat. Methods* **10**, 277–278 (2013). Medline doi:10.1038/nmeth.2406

42. R. Fitzhugh, Statistical Properties of the Asymmetric Random Telegraph Signal, with Applications to Single-Channel Analysis. *Math. Biosci.* **64**, 75–89 (1983). doi:10.1016/0025-5564(83)90028-7